⌘ *Author's Choice*

THE JOURNAL OF BIOLOGICAL CHEMISTRY VOL. 285, NO. 44, pp. 34048–34061, October 29, 2010

Structural and Functional Investigations of Matrilin-1 A-domains Reveal Insights into Their Role in Cartilage ECM Assembly*[S]

Received for publication, June 14, 2010, and in revised form, July 30, 2010 Published, JBC Papers in Press, August 21, 2010, DOI 10.1074/jbc.M110.154443

Maryline Fresquet[‡], Thomas A. Jowitt[‡], Louise A. Stephen[‡], Joni Ylöstalo[§], and Michael D. Briggs[‡1]

From the [‡]Wellcome Trust Centre for Cell-Matrix Research, Faculty of Life Sciences, University of Manchester, Manchester M13 9PT, United Kingdom and the [§]Center for Gene Therapy, Tulane University Health Sciences, New Orleans, Louisiana 70123

Matrilin-1 is expressed predominantly in cartilage and co-localizes with matrilin-3 with which it can form hetero-oligomers. We recently described novel structural and functional features of the matrilin-3 A-domain (M3A) and demonstrated that it bound with high affinity to type II and IX collagens. Interactions preferentially occurred in the presence of Zn^{2+} suggesting that matrilin-3 has acquired a requirement for specific metal ions for activation and/or molecular associations. To understand the interdependence of matrilin-1/-3 hetero-oligomers in extracellular matrix (ECM) interactions, we have extended these studies to include the two matrilin-1 A-domains (*i.e.* M1A1 and M1A2 respectively). In this study we have identified new characteristics of the matrilin-1 A-domains by describing their glycosylation state and the effect of *N*-glycan chains on their structure, thermal stability, and protein-protein interactions. Initial characterization revealed that *N*-glycosylation did not affect secretion of these two proteins, nor did it alter their folding characteristics. However, removal of the glycosylation decreased their thermal stability. We then compared the effect of different cations on binding between both M1A domains and type II and IX collagens and showed that Zn^{2+} also supports their interactions. Finally, we have demonstrated that both M1A1 domains and biglycan are essential for the association of the type II·VI collagen complex. We predict that a potential role of the matrilin-1/-3 hetero-oligomer might be to increase multivalency, and therefore the ability to connect various ECM components. Differing affinities could act to regulate the integrated network, thus coordinating the organization of the macromolecular structures in the cartilage ECM.

Matrilin-1 (cartilage matrix protein) was first identified as one of the major constituents of the cartilage proteoglycan mixture (1, 2). Subsequently, three other members of the matrilin protein family were identified and extensively characterized (3). Matrilin-1 is expressed predominantly in cartilage, in particular the growth plate and articular cartilages, and co-localizes with matrilin-3 with which it can form hetero-oligomers (4, 5). Matrilin-1 is primarily expressed in the maturation zone of the growth plate, whereas matrilin-3 is found mainly in the proliferation zone (6, 7).

Matrilin-1 and -3 are non-collagenous proteins with common modular features; matrilin-1 is composed of two von Willebrand factor A-domains (or A-domain; M1A1 and M1A2),[2] a single epidermal growth factor (EGF) domain, and a coil-coiled oligomerization domain, whereas matrilin-3 contains a single A-domain (M3A) and four EGF domains (8). All three A-domains (M1A1, M1A2, and M3A) possess metal ion-dependent adhesion site (MIDAS) motifs. Mutation of the MIDAS motif in either of the matrilin-1 A-domains have been shown to abolish filamentous network formation, suggesting that cation binding by the A-domains may be required for their function (9).

Matrilin-1 has also been shown to form disulfide-bonded oligomers with matrilin-3 in bovine cartilage extracts (4, 5). Furthermore, *in vitro* studies demonstrated that the predominant matrilin-1/-3 co-assembly was made up of two matrilin-1 monomers and two matrilin-3 monomers identical to the hetero-oligomers identified *in vivo* (6, 10). The M1A2 domain has been shown to regulate multimerization of the matrilin-1 protein (9, 11), such that deletion of the M1A2 domain converted the trimeric matrilin-1 protein into a mixture of monomers, dimers, and trimers, whereas deletion of the M1A1 domain did not affect the trimeric conformation (9, 11).

The formation of matrilin-1/matrilin-3 hetero-oligomers (4, 7, 10), in combination with proteolytic processing (11, 12), results in widespread molecular heterogeneity and therefore provides a rich array of potential sites of interaction. The variable multivalency of matrilin-1/-3 hetero-oligomers could possibly mediate interactions in the extracellular matrix (ECM) and effect its macromolecular structure and overall stability. The physical properties of the cartilage ECM depends on the molecular characteristics and the supramolecular assembly of its constituents, primarily collagens, proteoglycans, and bridging molecules such as COMP and the matrilins. It has already been established that a potential function for the matrilin proteins is to modulate collagen network organization (13, 14).

We have now studied this role in more detail by examining directly the interactions between type II collagen, the main struc-

* This work was supported in part by Grants 071161/Z/03/Z and 084353/Z/07/Z from the Wellcome Trust.

⌘ *Author's Choice*—Final version full access.

[S] The on-line version of this article (available at http://www.jbc.org) contains supplemental Figs. S1–S3.

[1] Recipient of a Wellcome Trust Senior Research Fellowship in Basic Biomedical Science. To whom correspondence should be addressed: Michael Smith Bldg., Oxford Road, Manchester M13 9PT, United Kingdom. Tel.: 44-161-275-5642; Fax: 44-161-275-5082; E-mail: mike.briggs@manchester.ac.uk.

[2] The abbreviations used are: M1A, matrilin-1 A-domain; M3A, matrilin-3 A-domain; MALLS, multiangle laser light scattering; MIDAS, metal ion-dependent adhesion site; ECM, extracellular matrix; SPR, surface plasmon resonance; QCM-D, quartz crystal microbalance with dissipation.

tural component of cartilage, and the three individual A-domains of matrilin-1/-3 (namely M1A1, M1A2, and M3A). We have also investigated the binding characteristics of the three A-domains with type IX collagen, which acts to link type II collagen fibrils together. To refine a model of ECM assembly, we monitored in real time the protein network formed by type VI collagen, biglycan, matrilin-1 A1-domain, and type II collagen.

In summary, this current study focuses primarily on characterizing the structure of the individual matrilin-1 A-domains and analyzing their interactions with other proteins of the cartilage ECM. These data will help in understanding further the role that multivalency plays in the functioning of matrilin-1/3 hetero-oligomers.

EXPERIMENTAL PROCEDURES

Cloning and Sequencing of Human Matrilin-1 A-domains—The matrilin-1 A1 and A2 domains were amplified from a full-length human cDNA clone by PCR and subcloned into the pSecTagA vector between SfiI and XhoI restriction sites of the multiple cloning site. These cDNA fragments were then re-amplified by PCR. The forward primer encompassed the first 20 nucleotides (from the ATG start codon upstream of the Ig κ-chain secretion signal) found in pSecTag and included a NotI restriction site (primer 5′-gcggccgcatggagacagacacact-3′). The reverse primers also contained an engineered NotI cleavage site in addition to an in-frame FLAG tag (sequence, DYKDDDDK) (5′-gcggccgctcacttatcgtcgtcatccttgtaatcgtctgacaccacgcagaaggcc-3′ for M1A1 and 5′-gcggccgctcacttatcgtcgtcatccttgtaatcgtcttcctccacacagatctt-3′ for M1A2). PCR products were subcloned using the TA Cloning method (Invitrogen), digested with the restriction enzyme NotI, cloned into the pCEP4 expression vector (Invitrogen), and sequenced. A single correct clone for each construct (pCEP4-M1A1 and pCEP4-M1A2) was used for all subsequent experiments.

Site-directed Mutagenesis—To abolish the *N*-glycosylation sites, the asparagine residue from the recognition motifs (N*X*T/S) was mutated to an alanine. PCR-based site-directed mutagenesis was performed on both wild type pCEP4-M1A1 and pCEP4-M1A2 clones using the following primer pairs: 5′-gacgtggggccc**gc**tgccacccgggtg-3′ and 5′-cacccgggtggc**agc**gggcccccacgtc-3′ for M1A1; 5′-gcggctgtgcgg**gc**tatgtcctacatg-3′ and 5′-catgtaggacat**agc**ccgcacagccgc-3′ for M1A2. The relevant amino acid codons are indicated in bold and the mutated nucleotides are underlined.

Matrilin-1 A-domains Protein Preparation—Recombinant human M1A1 and M1A2 domains were expressed as secreted proteins by 293-EBNA cells, affinity purified using the incorporated FLAG tag, and subjected to size-exclusion chromatography as described previously (15). The purity of the recombinant proteins was checked by silver staining of the gel. The identity of the recombinant proteins was confirmed by peptide mass mapping of excised band using electrospray ionization (ESI) tandem mass spectrometry.

PNGase Digest—0.5 μg of recombinant proteins were treated with 0.01 unit of PNGase F (QA Bio) for 48 h at 37 °C, and the treated protein products were analyzed by SDS-PAGE.

Homology Modeling—The amino acid sequence of each A-domain from human matrilin-1 was used to search the Swiss Model data base (EXPASY). Protein sequences resulting from this search included human von Willebrand factor A1 and A3 domains and the integrin I-domain. The sequence with the highest homology was the von Willebrand factor A3 (PBD code 1ao3-A) and this structure was used for homology modeling. The secondary structural elements from the von Willebrand factor A3 and the matrilin-1 A-domains were overlaid on a sequence alignment (using PYMOL), which located the asparagine residue involved in the glycosylation site of the proteins. The models of the matrilin-1 A-domains were built based on the coordinates of von Willebrand factor A3.

Structural Characterization by MALLS and CD—Samples of purified recombinant protein were subjected to Multiangle Laser Light Scattering (MALLS) analysis and applied to a Superdex 75 gel filtration column (GE Healthcare). Light scattering intensity and eluant refractive index were analyzed using ASTRA version 5.21 software to give a weight-averaged molecular mass (M_w). The secondary structures of the proteins variants were then recorded using a Jasco-810 spectropolarimeter. Circular dichroism (CD) spectra were deconvoluted using CDSSTR software program. Both techniques have been described elsewhere in more detail (15).

Assessing the Thermodynamic Stability by Differential Scanning Calorimetry—The denaturation temperatures of all proteins variants were measured using differential scanning calorimetry (VP-DSC MicroCalorimeter, MicroCal Inc.), as described (15). The denaturation curves were fitted to a non-two-state model yielding the T_m.

Surface Plasmon Resonance—The binding ability of recombinant matrilin-1 A-domains to type II (Calbiochem) and type IX collagen (15) was tested on a Biacore 3000 instrument using a CM5 sensor chip. In the first instance, the Biacore was used to investigate the effect of cations on binding between both M1A domains and bovine type II and human type IX collagens. Freeze-dried collagens were re-dissolved in 500 mM acetic acid at a concentration of 1 mg/ml, then diluted to a concentration of 10 μg/ml in 10 mM Tris, pH 7.4, 150 mM NaCl containing either 1 mM Zn^{2+}, Mg^{2+}, and Mn^{2+} or 1 mM EDTA. These samples were injected over immobilized M1A1 (~1000 response units bound) or M1A2 (~700 response units bound) for 3 min at a flow rate of 30 μl/min.

Kinetic runs were also performed with type II and IX collagens using TBS running buffer containing 1 mM Zn^{2+}. The method used was the same as described previously (15). The kinetic analysis was determined on the BIAevalution 4.1 software.

Quartz Crystal Microbalance with Dissipation (Q-sense)—The kinetics of the binding between wild type and the unglycosylated forms of matrilin-1 and -3 A-domains and type II collagen were also determined using quartz crystal microbalance with dissipation (QCM-D) as an alternative to the surface plasmon resonance (SPR) method (BIAcore). QCM-D simultaneously monitors changes in resonance frequency (Δf) and dissipation (ΔD) in real time. Δf primarily measures changes in the mass attached to the oscillating sensor surface (a silicon dioxide crystal in this case), whereas ΔD measures properties related to the viscoelasticity of the adsorbed layer (a network of type II collagen) (16).

Characterization of Matrilin-1 A-domains

All QCM-D measurements were performed with a Q-Sense E1 System at a temperature of 20.0 °C. A SiO_2-coated crystal (Q-sense AB) with a fundamental resonance frequency (*f5*) of 5 MHz was equilibrated in the running buffer (10 mM Tris, pH 7.4, 150 mM NaCl, 1 mM Zn^{2+}). 50 μg/ml of type II collagen (diluted in the same running buffer) was then adsorbed at a flow rate of 100 μl/min until saturation (~3 h).

The kinetic evaluation of the interactions between type II collagen and the matrilin A-domains was performed by exposing the immobilized collagen to a series of successively increasing concentrations of: 1) matrilin-3 A-domain (0, 90.78, 181.56, 272.34, 363.12, 453.91, and 680.86 nM); 2) matrilin-1 A1 (0, 88.1, 176.21, 264.32, 352.42, 440.53, and 660.79 nM); and 3) matrilin-1 A2 (0, 86.6, 173.16, 259.74, 346.32, 432.9, and 649.35 nM). After each of the concentration steps, the bound proteins were eluted with TBS containing 1 mM EDTA and allowed to stabilize in the running buffer before passing over the next concentration. All the experiments were repeated three times.

The maximum association rate (or V_{max}) for each concentration was derived using the following Hill equation (equivalent to Langmuir equation),

$$y = V_{max} \frac{x^n}{k^n + x^n} \quad \text{(Eq. 1)}$$

where y is the measured frequency change, x the time (s), and k is the Michaelis constant. In this case, $n = 1$, which corresponds to a non-cooperative reaction (the affinity between the two proteins is not dependent on whether or not other ligand molecules are already bound). The matrilin A-domain binding (or affinity) was then determined by plotting each calculated V_{max} as a function of increasing analyte concentrations (supplemental Figs. S2) and fitted to the same model generating the K_D (the equilibrium dissociation constant). This non-linear curve fitting method was performed using OriginPro8 software.

A different approach was employed to compare the behaviors of all A-domains variants following binding to type IX collagen. A solution of 10 μg/ml of type IX collagen was immobilized onto the crystal surface until it reached saturation. Then 5 μg/ml of each matrilin A-domain was sequentially injected and each experiment was repeated three times. The proteins concentrations were determined spectrophotometrically using extinction coefficients at 280 nm of 0.411 for M3A, 0.265 for M1A1, and 0.463 for M1A2.

This technique was also used to study complex formation between type VI collagen (Chemicon), biglycan (a kind gift from Prof. P. Bishop), matrilin-1 A-domains, and type II collagen in real time. Prior to type VI collagen adsorption, the crystal was brought into contact with TBS containing 1 mM Zn^{2+} to establish a baseline. 10 μg/ml of the collagen was then immobilized onto the surface until saturation. A succession of 5 μg/ml of biglycan, M1A1, M1A2, and type II collagen was then injected to form the complex. All proteins were diluted in the same running buffer (TBS + 1 mM Zn^{2+}). Western blotting was performed using antibodies to type VI collagen (Chemicon), biglycan (Abcam), matrilin-1 A-domains (anti-FLAG, Sigma), and type II collagen (Chemicon).

RESULTS

Evolutionary Relationship of the Matrilin A-domains—Understanding the sequence relationship between the different A-domains of the matrilin protein family can unravel the evolutionary history of these proteins as well as provide information about their potential function. For example, it has been previously proposed by Deák *et al.* (8) that all of the matrilin proteins evolved from a common ancestor. This suggestion is based on the observation that they all comprise at least one vWFA domain (or A-domains), a variable number of EGF-like repeats and a single coil-coiled oligomerization domain. However, during evolution the matrilin-3 A-domain closest to the coil-coiled domain is believed to have been lost (8) (Fig. 1*A*). The significant sequence similarity between the single matrilin-3 A-domain and the matrilin-1 A1-domain (Fig. 1*B*; 62% sequence homology) implies that they have the same evolutionary origin and possibly the same structure and function. In contrast, the matrilin-3 A-domain and the matrilin-1 A2-domain are more distantly related and share only 41% sequence homology (Fig. 1*B*).

The amino acid sequence alignments of M3A, M1A1, and M1A2 also reveal that all three proteins possess a signature sequence, D*X*S*X*S...(T/S)...D, referred to as the MIDAS motif as described previously (8, 17) (Fig. 1*C*). Furthermore, both M1A1 and M1A2 proteins contain a potential glycosylation directing sequence defined by the sequons NAT for M1A1 and NMS for M1A2 (Fig. 1*B*). Multiple sequence alignment of M1A1 sequences revealed conserved *N*-linked glycosylation sites in human, mouse, and chick. M1A2 sequences showed conserved *N*-linked glycosylation sites only in human and mouse but not in chick. Moreover both matrilin-1 A-domains lack the *N*-glycosylation site in zebrafish (Fig. 1*C*).

Structural Characteristics of Recombinant Matrilin-1 A-domains—Matrilin-1 A-domains (M1A1 and M1A2) were purified as secreted proteins and appeared as doublets with an apparent molecular mass under denaturing conditions of ~25 kDa according to SDS-PAGE (Fig. 2*A*). Tryptic peptide analysis by ESI tandem mass spectrometry validated the identity of both doublets as M1A1 and M1A2, respectively (not shown). Our finding that both A-domains ran as doublets prompted us to hypothesize that the lower bands were the unglycosylated forms, whereas the upper bands were the glycosylated forms of the proteins. This hypothesis was supported by the observation that both protein sequences contain a potential *N*-glycosylation site (Fig. 1*C*). A homology model of the M1A1 domain located the only possible *N*-glycosylation site at the opposite face to the MIDAS motif, whereas the only possible *N*-glycosylation site of the M1A2 domain was situated on the α2 helix (Fig. 2*B*).

An *N*-glycanase digestion performed on the purified proteins showed that both doublets became a sharper single band, confirming that a proportion of the molecules were glycosylated (Fig. 2*C*). Interestingly, the M1A1 domain appeared mostly glycosylated (with a relative amount of 70% of glycosylated species against 30% of unglycosylated quantified using densitometry), whereas the M1A2 domain contained a comparable proportion of glycosylated and unglycosylated protein (50% of glycosylated

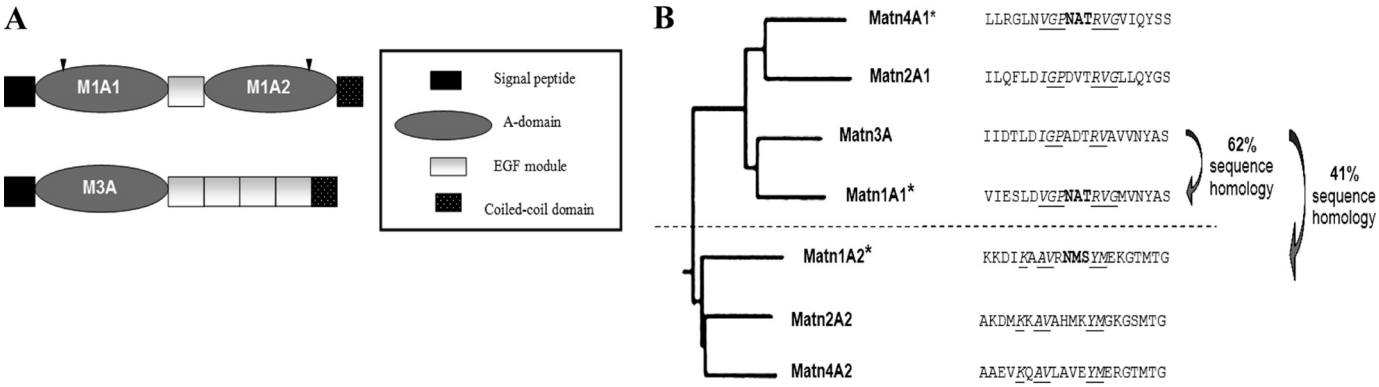

C

```
MATN1A1_HUMAN      ----CRTRPTDLVFVVDSSRSVRPVEFEKVKVFLSQVIESLDVGPNATRVGMVNYASTVK 56
MATN1A1_MOUSE      ----CRTRPTDLVFVVDSSRSVRPVEFEKVKVFLSQVIESLDVGPNATRVGLVNYASTVK 56
MATN1A1_CHICK      ----CRTKPTDLVFIIDSSRSVRPQEFEKVKVFLSRVIEGLDVGPNSTRVGVINYASAVK 56
MATN1A1_DANRE      ----CNTKPTDVVFIVDSSRSVRPSEFEQVKVFLAKVIDGLSVGPDATRVGVVNYASRVK 56

MATN3_HUMAN        ----CKSRPLDLVFIIDSSRSVRPLEFTKVKTFVSRIIDTLDIGPADTRVAVVNYASTVK 56
MATN3_MOUSE        ----CKSRPLDLVFIIDSSRSVRPLEFTKVKTFVSRIIDTLDIGATDTRVAVVNYASTVK 56
MATN3_CHICK        ----CKNRPLDLVFIIDSSRSVRPEEFEKVKIFLSKMIDTLDVGERTTRVAVMNYASTVK 56
MATN3a_DANRE       ----CRSRPLDLVFIIDSSRSVRPGEFEKVKIFLADMVDTLDVGPDATRVAVVNYASTVK 56
MATN3b_DANRE       ----CKSRPLDLVFIIDSSRSVRPAEFEKVKIFLSEMVDSLDIGSDATRVALVNYASTVN 56

MATN1A2_HUMAN      CSGGGGSSATDLVFLIDGSKSVRPENFELVKKFISQIVDTLDVSDKLAQVGLVQYSSSVR 60
MATN1A2_MOUSE      CRGGGSGSATDLVFLIDGSKSVRPENFELVKKFINQIVDTLDVSDRLAQVGLVQYSSSIR 60
MATN1A2_CHICK      CSGG-SGSALDLVFLIDGSKSVRPENFELVKKFINQIVESLEVSEKQAQVGLVQYSSSVR 59
MATN1A2_DANRE      ----CSNAATDVVFLIDGSKSVRPENFELVKKWINLIIDKLDVSETNTHVGLVQYSSTVK 56
                           . *:**::*.*:**** :*  ** ::  ::: *.:.   ::*.:::*:* :.

MATN1A1_HUMAN      QEFSLRAHVSKAALLQAVRRIQPLSTGTMTGLAIQFAITKAFGDAEGGRSRSPDISKVVI 116
MATN1A1_MOUSE      PEFPLRAHGSKASLLQAVRRIQPLSTGTMTGLALQFAITKALSDAEGGRARSPDISKVVI 116
MATN1A1_CHICK      NEFSLKTHQTKAELLQAVQRIEPLSTGTMTGLAIQFAISRAFSDTEGARLRSPNINKVAI 116
MATN1A1_DANRE      NEVSLKSHKTKAALVKAVSKIEPLSTGTMTGLAIQFAMNVAFSEAEGGR-KSPDISKVAI 115

MATN3_HUMAN        IEFQLQAYTDKQSLKQAVGRITPLSTGTMSGLAIQTAMDEAFTVEAGAREPSSNIPKVAI 116
MATN3_MOUSE        IEFQLNTYSDKQALKQAVARITPLSTGTMSGLAIQTAMEEAFTVEAGARGPMSNIPKVAI 116
MATN3_CHICK        VEFPLRTYFDKASMKEAVSRIQPLSAGTMTGLAIQAAMDEVFTEEMGTRPANFNIPKVVI 116
MATN3a_DANRE       IEFLLKSHLTKDTIKQAITRIEPLAAGTMTGMAIKKAMDEAFTEKSGARPKSKNISKVAI 116
MATN3b_DANRE       IEFHLKKYFSKAEVKQAFSRIDPLSTGTMTGMAIKTAMEQVFTENAGARPLKKGIGKVAI 116

MATN1A2_HUMAN      QEFPLGRFHTKKDIKAAVRNMSYMEKGTMTGAALKYLIDNSFTVSSGAR---PGAQKVGI 117
MATN1A2_MOUSE      QEFPLGRFHSKKDIKARVRNMSYMEKGTMTGAALKYLIDNSFTVSSGAR---PGAQKVGI 117
MATN1A2_CHICK      QEFPLGQFKNKKDIKAAVKKMAYMEKGTMTGQALKYLVDSSFSIANGAR---PGVPKVGI 116
MATN1A2_DANRE      QEFPLGRHNSKRSLKEAVKRMNYMERGTMTGHALSFLVDNSFGPNQGAR---PGVPKVGI 113
                    *. *  .  *  :   . .:  :  ***:* *:.  :   :    * *    .  ** *

MATN1A1_HUMAN      VVTDGRPQDSVQDVSARARASGVELFAIGVGSVDKATLRQIASEPQDEHVDYVESYSVIE 176
MATN1A1_MOUSE      VVTDGRPQDSVRDVSERARASGIELFAIGLGRVDKATLRQIASEPQDEHVDYVESYNVIE 176
MATN1A1_CHICK      VVTDGRPQDGVQDVSARARQAGIEIFAIGVGRVDMHTLRQIASEPLDDHVDYVESYSVIE 176
MATN1A1_DANRE      IVTDGRPQDNIRDIAARAREAGIEIFAIGVGRVDMTTLRQMASEPLEDHVDYVESYSLIE 175

MATN3_HUMAN        IVTDGRPQDQVNEVAARAQASGIELYAVGVDRADMASLKMMASEPLEEHVFYVETYGVIE 176
MATN3_MOUSE        IVTDGRPQDQVNEVAARARASGIELYAVGVDRADMESLKMMASKPLEEHVFYVETYGVIE 176
MATN3_CHICK        IVTDGRPQDQVENVAANARTAGIEIYAVGVGRADMQSLRIMASEPLDEHVFYVETYGVIE 176
MATN3a_DANRE       IVTDGRPQDQVEEVSAAARASGIEIYAVGVDRADMRSLKLMASNPLEDHVFYVETYGVIE 176
MATN3b_DANRE       IVTDGRPQDKVEEVSAAARASGIEIYAVGVDRAEVRSLKQMASQPLDDHVFYVETYGVIE 176

MATN1A2_HUMAN      VFTDGRSQDYINDAAKKAKDLGFKMFAVGVGNAVEDELREIASEPVAEHYFYTADFKTIN 177
MATN1A2_MOUSE      VFTDGRSQDYINDAARKAKDLGFKMFAVGVGNAVEEELREIASEPVADHYFYTADFKTIN 177
MATN1A2_CHICK      VFTDGRSQDYITDAAKKAKDLGFRMFAVGVGNAVEDELREIASEPVAEHYFYTADFRTIS 176
MATN1A2_DANRE      VFTDGRSQDYIGDAAKKAKALGFKMYAVGVGNAVEDELREIASEPIADHYFYTADFKTMN 173
                   :.****.** : : :  *:  *..::*:*:. .    *: :**:*  :*  *.  :  :.

MATN1A1_HUMAN      KLSRKFQEAFC 187
MATN1A1_MOUSE      KLAKKFQEAFC 187
MATN1A1_CHICK      KLTHKFQEAFC 187
MATN1A1_DANRE      KLTKKFQEAFC 186

MATN3_HUMAN        KLSSRFQETFC 187
MATN3_MOUSE        KLSARFQETFC 187
MATN3_CHICK        KLTSKFRETFC 187
MATN3a_DANRE       KLTSKFRETLC 187
MATN3b_DANRE       KLTSKFRETLC 187

MATN1A2_HUMAN      QIGKKLQKKIC 188
MATN1A2_MOUSE      QIGKKLQKQIC 188
MATN1A2_CHICK      NIGKKLQMKIC 187
MATN1A2_DANRE      QIAKKLQINVC 184
                   ::  :::  .*
```

FIGURE 1. **Phylogenetic relationship between the matrilin-1 and matrilin-3 A-domains.** *A*, the modular structures of matrilin-1 and matilin-3 monomers. The *black arrows* show the location of the potential glycan chain attachment site in the A-domains of matrilin-1. *B*, phylogenetic tree of human matrilin A-domains. The *length of the horizontal lines* is proportional to the evolutionary distance between the sequences. *Asterisks* indicate the A-domains with a potential *N*-linked glycosylation site, which is also shown in *bold* on the amino acid sequence. The *underlined residues* show the similarity in sequence around the *N*-glycosylation site across the different A-domains. *C*, multiple sequence alignment from a set of selected species of matrilin-1 and -3 A-domains. *, indicates the residues that are identical in all sequences in the alignment; *colons* and *dots* represent conserved and semi-conserved substitutions, respectively. The potential *N*-linked glycosylation sites are shown in *bold* and the residues that comprise the MIDAS motif are highlighted in *gray*.

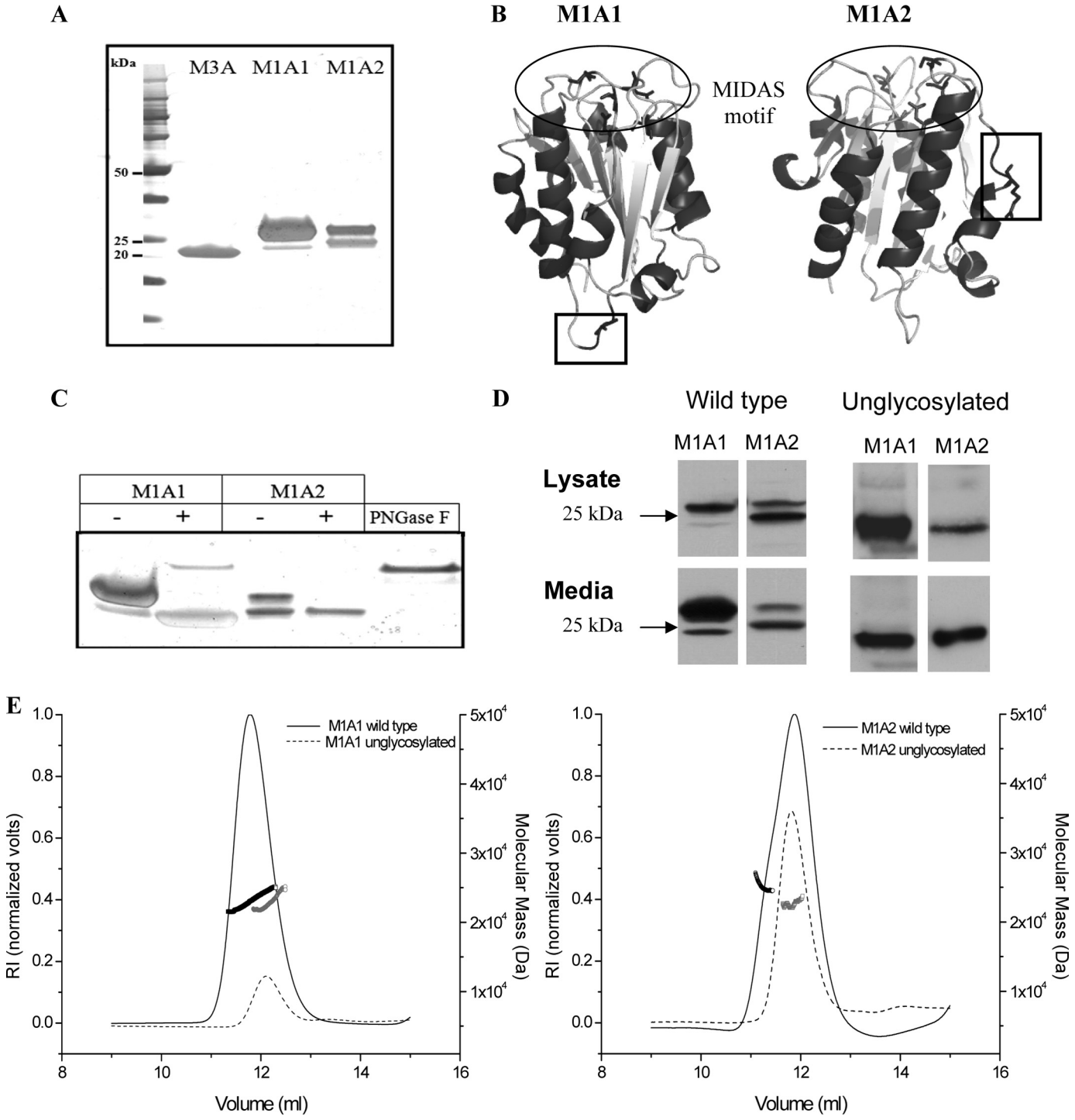

FIGURE 2. **Purification and characterization of recombinant matrilin-1 A-domains.** *A,* silver-stained SDS-PAGE gel of purified recombinant matrilin-1 and -3 A-domains under reducing conditions; *lane 1*, molecular weight marker; *lane 2*, purified recombinant matrilin-3 A-domain, which is resolved as a single band of ~ 22 kDa; *lanes 3* and *4*, purified matrilin-1 A1 (*M1A1*) and A2 (*M1A2*) domains, respectively, which appeared as doublets with a molecular mass ~25 kDa. *B*, homology models of the matrilin-1 A-domains indicating the positions of the potential *N*-glycosylation sites on both molecules. Homology model of the M1A1 domain locating the only possible *N*-glycosylation site (*boxed*) on the opposite face to the MIDAS motif (*circled*). Homology model of M1A2 domain showing the only possible *N*-glycosylation site (*boxed*) situated on the α2 helix. Pictures were generated using PYMOL based on template PDB code 1ao3-A (A3 domain of Von Willebrand factor). *C*, silver-stained gel of *N*-glycanase digests of purified M1A1 and M1A2 domains. Following treatment with PNGase F (+) only the lower band is apparent in each case. *D*, the effect of glycosylation on the secretion of the proteins. SDS-PAGE and Western blot analysis under reducing conditions of cell lysates and conditioned medium from 293-EBNA cells transfected with the matrilin-1 A-domains. Wild type (glycosylated, *left panel*) and the mutated (unglycosylated, *right panel*) constructs. The *arrow* indicates the position of the 25-kDa marker. *E*, structural analysis of matrilin-1 A-domains in solution. Superdex 75 gel filtration chromatography and MALLS analysis of recombinant wild type and unglycosylated matrilin-1 A-domains. The graph shows the elution position and molecular weight of the matrilin-1 A-domains obtained from MALLS experiments. The individual data points represent the molecular weight distribution across the peak in *black* for the wild type proteins and *gray* for the unglycosylated forms.

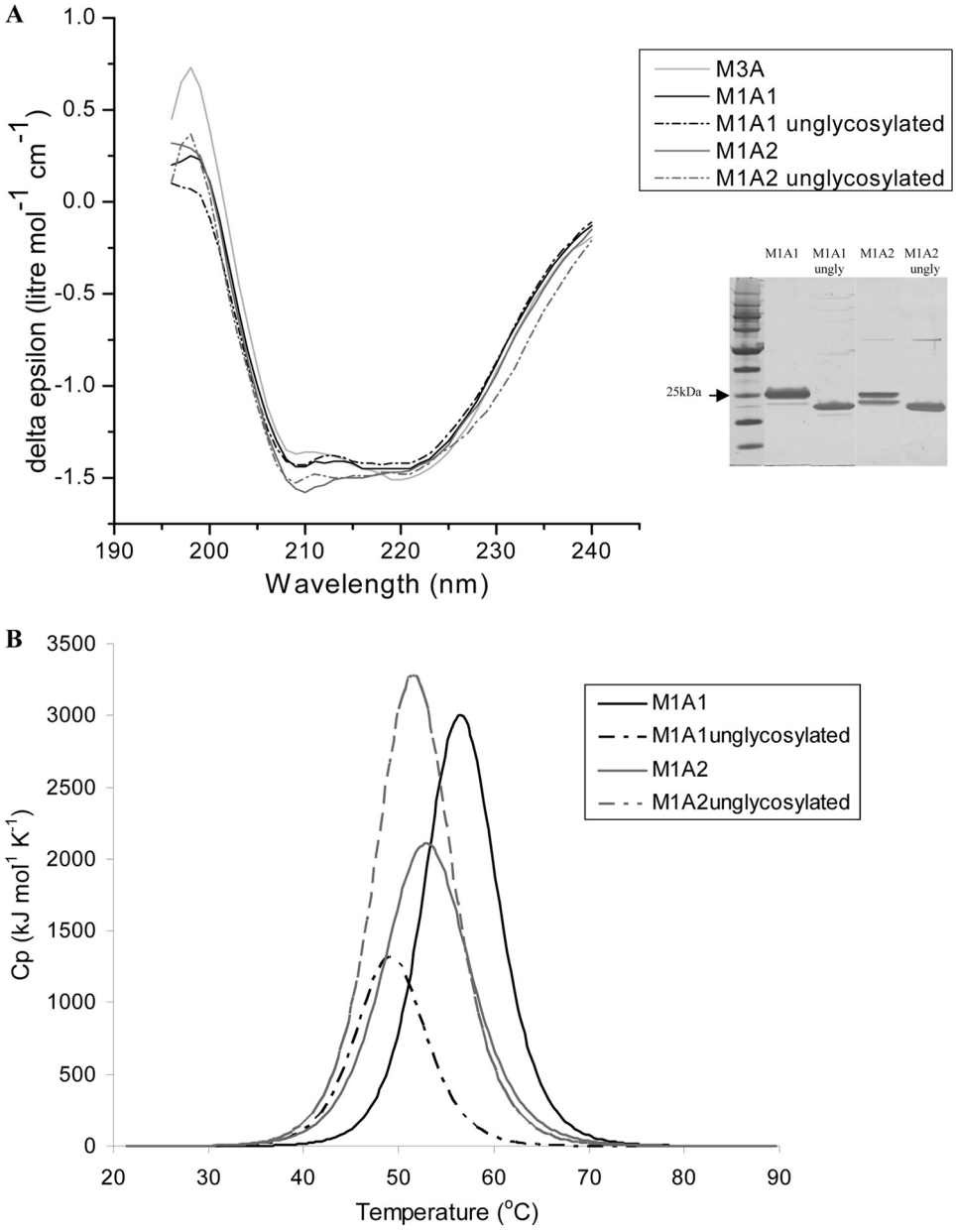

FIGURE 3. **Structural analysis of recombinant matrilin-1 A-domains, wild type (glycosylated) and unglycosylated.** *A*, the CD spectra of purified matrilin-1 and -3 A-domains were monitored between 190 and 240 nm in 20 mM Tris buffer, 150 mM NaCl, pH 7.4, at 25 °C. The purity of the recombinant proteins was verified by silver staining of SDS-PAGE gel under reducing conditions (*inset*). These data reveal that glycosylation in both matrilin-1 A-domains do not affect their secondary structures content with characteristic β-sheet and α-helical elements. *B*, thermal stability of recombinant matrilin-1 A-domains. The denaturation heat capacity curves were measured by differential scanning calorimetry. The differential scanning calorimetry profiles for wild type matrilin-1 A1 and A2 domains indicate a more stable conformation (*solid line*) compared with the unglycosylated forms (*dotted line*).

and 50% unglycosylated species). This suggested that both glycosylation-directing sequences of the matrilin-1 A-domains are accessible on the surface of the proteins, thereby allowing the attachment of *N*-glycan chains *in vitro*.

To determine the effect of glycosylation on the secretion of the recombinant proteins, mutant M1A1 and M1A2 domains were generated in which the *N*-glycosylation sites were abolished by replacing the appropriate asparagine residue with an alanine residue. The cell lysates and the conditioned medium were analyzed by SDS-PAGE and Western blotting (Fig. 2*D*), which confirmed that both of these unglycosylated proteins were secreted.

The wild type and unglycosylated proteins were then run on a size exclusion column coupled to a multiangle laser light scattering detector to determine their average molecular weights (M_r). The molecular mass of wild type M1A1 was calculated to be 23.4 kDa and the unglycosylated form to be 0.7 kDa smaller at 22.7 kDa (Fig. 2*E*; *left-hand panel*). The chromatograph for the M1A2 protein showed that it eluted in two peaks, which corresponded to the upper and lower bands of the doublet (Fig. 2*E, right-hand panel*). The first peak was defined as the glycosylated form of M1A2 and gave a molecular mass of 24.9 kDa. The elution position of the second peak of the protein overlaid perfectly with the one from the unglycosylated form and was found to be 1.8 kDa smaller at 23.1 kDa. These data derived from the light scattering experiments therefore supported our initial assessment that both domains possess one *N*-linked polysaccharide chain each.

Potential Roles of the Glycosylation in Matrilin-1 A-domains—To assess if glycosylation had any significant effect on the conformation of the A-domains, the secondary structure characteristics of the four proteins was determined by circular dichroism (CD). The M1A1 CD spectrum showed a slight decrease in the relative amounts of α-helix content and a subsequent increase in β-sheet elements compared with M1A2 (Fig. 3*A*). This was confirmed by calculating the average values for secondary structure composition following CDSSTR analysis. The M1A1 domain was found to be composed of 9% α-helix, 36% β-sheet, 24% turn, and 31% random coil and the M1A2 domain of 15% α-helix, 30% β-sheet, 24% turn, and 31% random coil. Moreover, both matrilin-1 A-domains exhibited a smaller β-strand proportion and a greater α-helical content than the matrilin-3 A-domain (15). These data also revealed that there was no significant difference in the secondary structure between the wild type and unglycosylated forms of the proteins suggesting that glycosylation does not affect the folding of the individual domains.

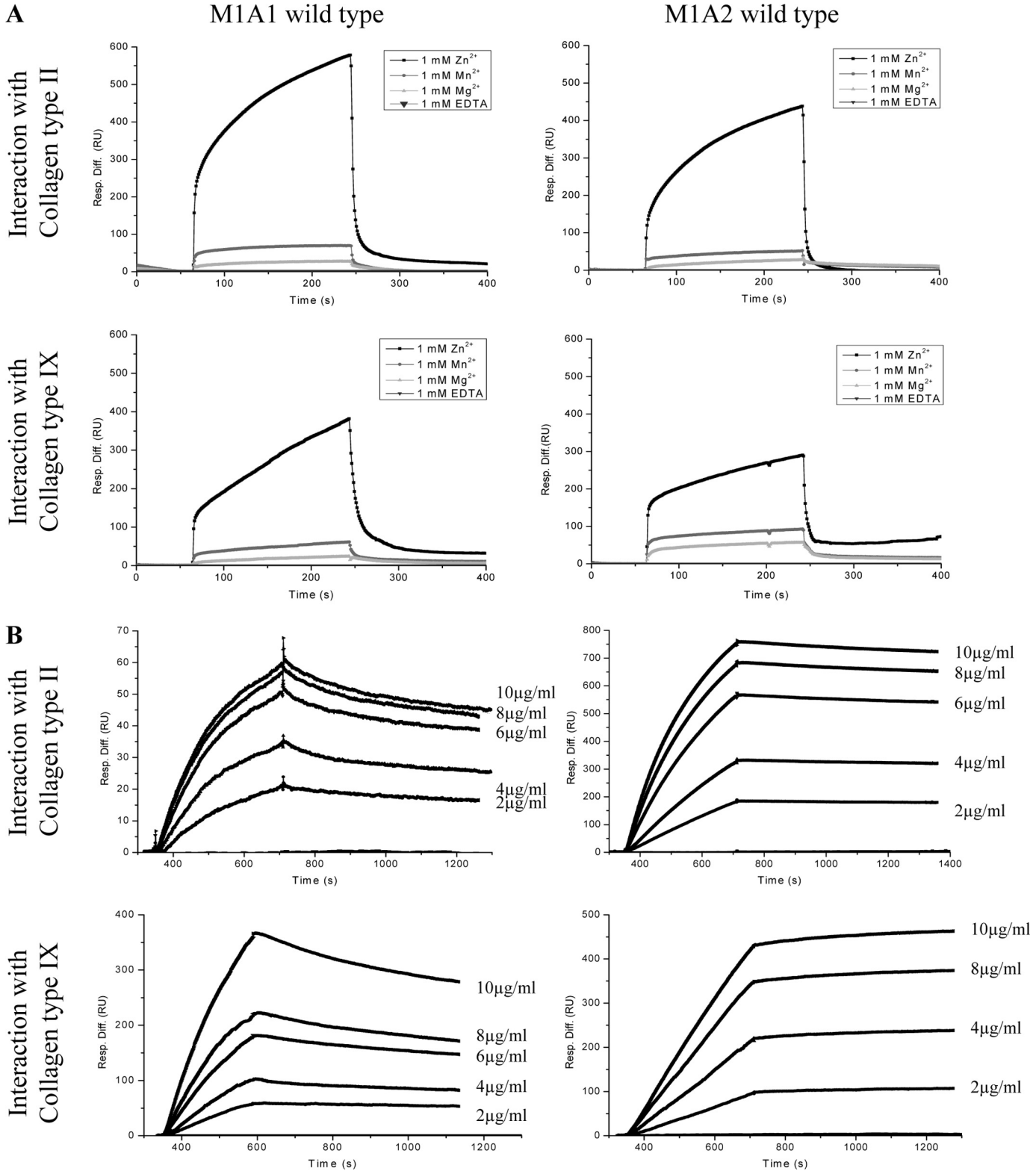

	matn3A	matn1A1	matn1A2
Collagen type II	6.2 nM	8.8 nM	2.13 nM
Collagen type IX	1.5 nM	4.4 nM	N/D

Glycosylation can also influence the behavior of a protein whereby the addition of the *N*-glycans can decrease the amino acid core flexibility resulting in an increased thermal stability (18), perhaps in an attempt to increase protein longevity. To determine thermal stability of the matrilin-1 A-domains, differential scanning calorimetry was used. The denaturation temperature of the wild type M1A1 domain was within the temperature ranges of 56–57 and ~49 °C for the unglycosylated form (Fig. 3*B*). The thermal stability of the wild type and unglycosylated M1A2 domains was also assessed and the denaturation temperatures obtained were ~54 and 52 °C, respectively. These data revealed that the wild type forms of the proteins were indeed more resistant to thermal unfolding than the unglycosylated forms, which provides evidence that glycosylation has evolved to give some protection and durability to the proteins.

Zn^{2+} Is Required for the Binding of M1A1 and M1A2 to Collagen Types II and IX—We have recently shown that the matrilin-3 A-domain bound with high affinity to type II and type IX collagens in the presence of Zn^{2+} (15). We therefore compared the role of different cations (1 mM each of Zn^{2+}, Mn^{2+}, and Mg^{2+}) on the binding properties of the matrilin-1 A-domains using SPR (Fig. 4*A*). These studies demonstrated that whereas 1 mM Zn^{2+} supported strong binding of type II and IX collagens to the wild type M1A1 and M1A2 domains, in contrast, binding in the presence of 1 mM Mn^{2+} and Mg^{2+}, or 1 mM EDTA (used as control) was negligible or completely abolished. This suggests that all three individual A-domains (M3A, M1A1, and M1A2) have acquired specificity for Zn^{2+} binding.

Supramolecular Assembly of Matrilin-1 and -3 A-domains in the Cartilage Collagen Network; Binding of Matrilin-1 A-domains to Type II Collagen—The binding kinetics of the wild type and unglycosylated matrilin-1 A-domains to type II collagen was studied further by QCM-D to determine whether glycosylation influenced molecular associations. During the adsorption phase type II collagen caused an initial rapid frequency decrease (mass increase) followed by a slower frequency decrease as the crystal saturated (supplemental Fig. S1, *phase 1*). By using this technique we were able to form a stable layer-by-layer architecture of type II collagen molecules without loosing any activity (which was the case when using SPR). Type II collagen showed evidence of oligomerization on the surface of the chip in a similar way to collagen type I shown by Johansson *et al.* (21), with collagen II forming fibrils before laying flat on the surface with a layer depth of 85 nm (similar to that for a single fibril). The fibrillar collagen surface could be repeatedly regenerated by removal of bound proteins using 1 mM EDTA (supplemental Fig. S1, *phase 5*), thus enabling multiple matrilin A-domain binding experiments (supplemental Fig. S1, *phase 4*). Successive incubations with increasing amounts of the different matrilin A-domains (M3A, M1A1/M1A2 both wild type and unglycosylated) allowed us to determine their relative affinities for type II collagen.

The M1A2 domain showed the strongest affinity with a K_D of ~50 nM compared with M3A (~91 nM) and M1A1 (~104 nM) (Fig. 5*A*). This trend was in agreement with the calculated K_D as determined by SPR analyses, which were 2.13 nM for M1A2, 6.2 nM for M3A, and 8.8 nM for M1A1 (Fig. 4*B*, *top panel*, and *table*). The difference in binding between M1A2 and M3A was also statistically significant ($p < 0.001$). However, no difference was detected between wild type M1A2 and the unglycosylated form (probably due to the fact that wild type M1A2 contains a high proportion of unglycosylated protein resulting in a masking effect). An interesting finding was that the unglycosylated form of M1A1 bound more strongly to type II collagen than the wild type molecule. This suggests that the flexible *N*-glycan chains might partially hide the binding site for type II collagen, thus narrowing the location of the binding site for this molecule to the opposite face of the MIDAS motif (Fig. 2*D*).

Subsequent data analysis by plotting frequency and dissipation shifts enabled us to better understand the nature of the interaction between the matrilin-1 and -3 A-domains and type II collagen. A comparison of the change in resonance frequency (bound mass) *versus* time revealed a fast binding of all three matrilin A-domains to type II collagen (Fig. 5*B, top left panel*). Measurements of the damping effect (dissipation factor) during binding experiments between the matrilin A-domains and type II collagen suggested that the matrilin-1 A-domains formed a more rigid structure with type II collagen than M3A did (Fig. 5*B, bottom left panel*). By combining f and D data we were able to obtain information about structural changes of the collagen surface following the binding of the matrilin A-domains. It is evident from the plot (Fig. 5*B, right panel*) that the M1 A-domains and M3A affected the immobilized collagen layer in a very different way. When M3A was added it bound to type II collagen in such a way that the resulting complex was more flexible, which was reflected by a higher $\Delta D/\Delta f$ ratio than the M1 A-domains. In contrast, the lower $\Delta D/\Delta f$ ratio measured for the four M1 A-domains indicated a more rigid complex.

Interactions between the Matrilin-1 A-domains and Type IX Collagen—In this series of experiments we used QCM-D to investigate changes in frequency and energy dissipation during adsorption of the different matrilin A-domains to a SiO_2 surface covered with a stable film of type IX collagen with a thickness of 6.5 nm. From the Δf *versus* time plot it can be seen that the M3A domain had a faster association rate than the M1A1 and M1A2 domains (Fig. 5*C, top left panel*) (*i.e.* following addition of the M3A solution a rapid frequency decrease (mass increase) occurred). The adsorption kinetics of the wild type M1A1 and its unglycosylated form exhibited a difference in mass uptake as opposed to both variants of M1A2, which showed no difference. The ΔD *versus* time plot showed that dissipation increased with time meaning more energy was dissipated as more proteins were adsorbed (Fig. 5*C, bottom left panel*). This was especially the case for the M3A domain, but no

FIGURE 4. **Functional analysis of recombinant matrilin-1 A-domains.** *A*, SPR analysis showing the effect of different cations on the binding of type II and IX collagens to M1A1 and M1A2. Interactions of immobilized M1A1 and M1A2 to type II collagen (10 μg/ml) in the presence of 1 mM Zn^{2+}, Mn^{2+}, and Mg^{2+}, and 1 mM EDTA are shown in the *top panel* and binding to type IX collagen (10 μg/ml) in the presence of 1 mM Zn^{2+}, Mn^{2+}, and Mg^{2+}, and 1 mM EDTA are shown in the *bottom panel*. *B*, interactions between the immobilized wild type (glycosylated) forms of M1A1 and M1A2 domains with type II (*top panels*) and IX collagens (*bottom panels*), respectively, in the presence of 1 mM Zn^{2+} as detected by surface plasmon resonance. The *table at the bottom* summarizes the K_D values obtained after kinetic analysis using BIAevalution software. *N/D,* not determined due to no dissociation between M1A2 and type IX collagen.

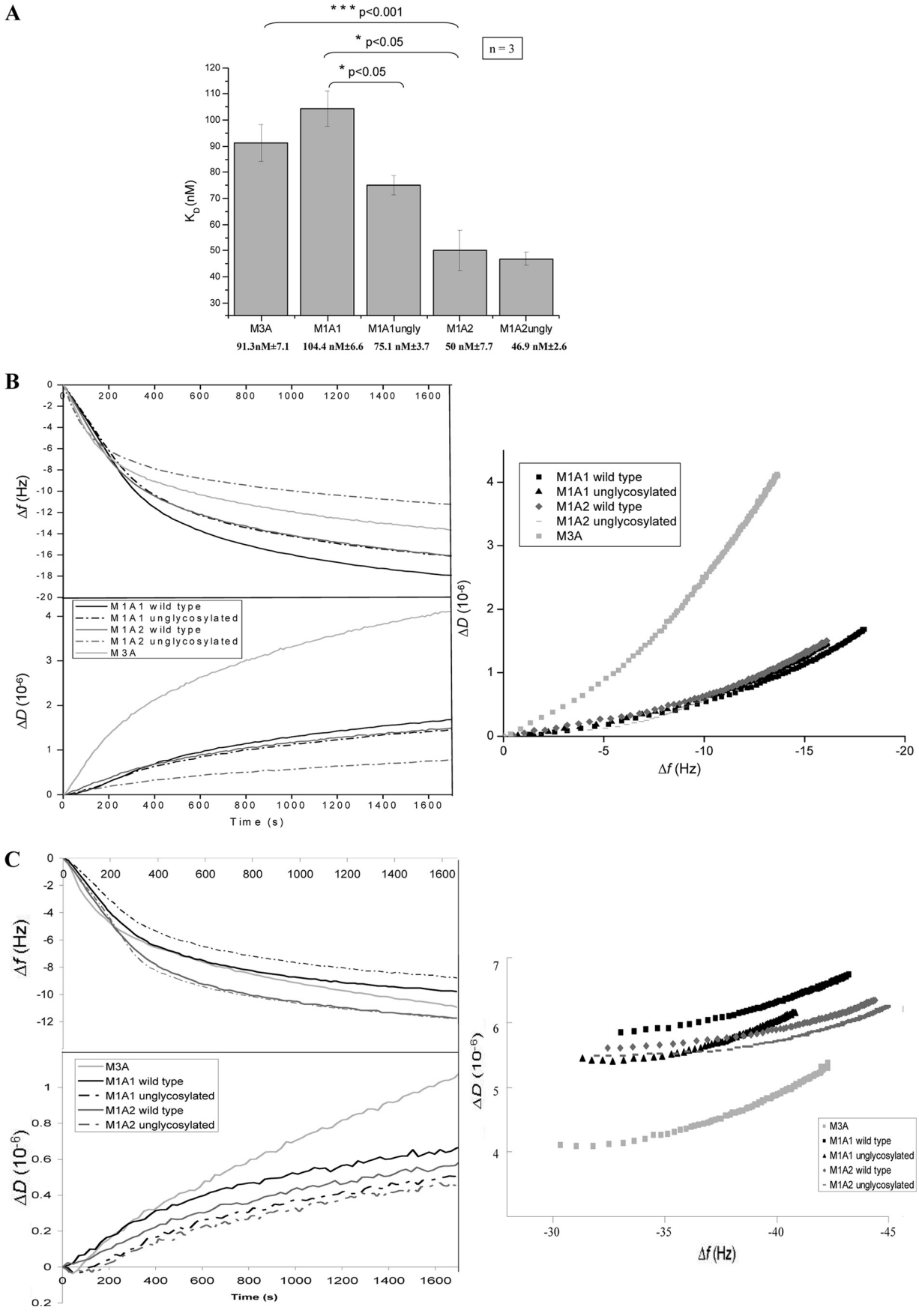
A
*** p<0.001
* p<0.05
* p<0.05
n = 3
K_D (nM)
M3A
M1A1
M1A1ungly
M1A2
M1A2ungly
91.3nM±7.1
104.4 nM±6.6
75.1 nM±3.7
50 nM±7.7
46.9 nM±2.6
B
Δf (Hz)
ΔD (10⁻⁶)
Time (s)
M1A1 wild type
M1A1 unglycosylated
M1A2 wild type
M1A2 unglycosylated
M3A
C
Δf (Hz)
ΔD (10⁻⁶)
Time (s)
M3A
M1A1 wild type
M1A1 unglycosylated
M1A2 wild type
M1A2 unglycosylated

significant differences in viscoelasticity of the different matrilin-1 A-domains could be observed. To correlate the observed changes in *f* and *D*, we plotted ΔD *versus* Δf, which does not take into account the time parameter (Fig. 5*C, right panel*). These data revealed differences between the adsorption behavior of the matrilin-3 A-domain and both of the matrilin-1 A-domains, which was not directly observed on the other plots. The different $\Delta D/\Delta f$ ratio can be divided into two groups; one for all of the matrilin-1 A-domains and the second one for the matrilin-3 A-domain alone, indicating at least two different kinetic processes occur during adsorption. The low $\Delta D/\Delta$f value for M3A suggests a strong binding to type IX collagen and also indicates that the addition of this molecule triggers a more rigid compact conformation of the type IX collagen layer. All four matrilin-1 A-domains share a similar, but higher ratio, suggesting that they form a more flexible structure and have a lower affinity for the layer below (*i.e.* type IX collagen). Further analysis of the curves for both M1A1 domains indicated that the wild type protein binds with slightly higher affinity (lower ratio), but again no difference could be detected between the two M1A2 proteins.

Protein Complex Formation between Type VI Collagen, Biglycan, the Matrilin-1 A-domains, and Type II Collagen Monitored in Real Time Using QCM-D—Type VI collagen has previously been shown to bind a wide range of proteins *in vitro*, such as the fibrillar type II collagen, and the proteoglycans biglycan and decorin (19). More recently Wiberg *et al.* (20) described the interaction between biglycan and matrilin-1 acting as a bridging complex with type II and VI collagens. In our study we monitored in real time the complex formation between type VI collagen, biglycan, the two matrilin-1 A-domains and type II collagen using QCM-D. In the first instance a layer of type VI collagen was deposited on the sensor surface in a random fashion corresponding to the sudden decrease in frequency (or increase in mass). Once a critical density had been reached, the collagen molecules most likely organized themselves into a stable and compact network, which was reflected by the small increase in frequency and decrease in dissipation (Fig. 6*A, phase 1*) as described elsewhere (21). The type VI collagen showed evidence of some oligomerization before forming a flat layer of 15 nm, which is consistent with an arrangement of triple helical molecules into filaments. Biglycan was then passed over the type VI collagen layer followed by the individual matrilin-1 A-domains (M1A1 first followed by M1A2; see Fig. 6*A, phase 2* and *3*, respectively). All 3 proteins showed the characteristics of binding (*i.e.* an increase in mass with a corresponding increase in dissipation). Finally, type II collagen was injected and bound to this complex (Fig. 6*A, phase 4*), which was characterized by a large shift in frequency and dissipation (due to the size of the collagen molecules).

At this stage in the experiment the protein complex was eluted from the crystal surface using SDS-PAGE loading buffer. The presence of the individual proteins in the complex was then confirmed by Western blotting using specific antibodies against type VI collagen, biglycan, matrilin-1 A-domains, and type II collagen (Fig. 6*B*). All of the individual proteins of the complex could be detected (*i.e.* types II and VI collagen and matrilin-1 A1-domain) with the exception of biglycan and matrilin-1 A2-domain. We subsequently detected biglycan following silver staining; however, M1A2 was not detectable, which led us to conclude that it was not part of the stable complex. We therefore performed the subsequent experiments with M1A1 alone.

To determine specificity of this protein assembly and complex formation, each protein of the complex was individually tested for binding against each of the other components (supplemental Fig. S3*A*). Biglycan and the matrilin-1 A1-domain individually bound to types II and VI collagen. Moreover, a pre-assembled type II collagen and matrilin-1 A1-domain complex interacted with biglycan, but not with type VI collagen. In a similar way, type II collagen and the biglycan complex associated with the matrilin-1 A1-domain, but not with type VI collagen. Interestingly, when type II collagen was absorbed onto the crystal no detectable direct binding with type VI collagen could be seen. However, in the reverse orientation we could observe a slight binding (3.5-fold less than in the complex) between type II collagen and type VI collagen. We therefore concluded from these data that both biglycan and the matrilin-1 A1 domain are required for the association of type VI collagen with type II collagen (supplemental Fig. 3*B*).

DISCUSSION

In this study we have determined novel characteristics of human recombinant matrilin-1 A-domains (M1A1 and M1A2, respectively) by describing their potential glycosylation state and the effect of the *N*-glycan chains on their structure, secretion, and protein-protein interactions *in vitro*.

Paulsson and Heinegård (2) first demonstrated that full-length matrilin-1 extracted from bovine tracheal cartilage contained 3.9% (w/w) carbohydrates. An amino acid sequence alignment of both human and bovine matrilin-1 revealed only two potential glycosylation-directing sequons, one being in the first A-domain (M1A1) and the other in the second A-domain (M1A2), suggesting that the human matrilin-1 A-domains are likely to be glycosylated *in vivo*. We have confirmed that both of these sites are glycosylated *in vitro* and that this post-translational modification by *N*-glycosylation was found to affect the biochemical properties of the M1A1 domain. The attachment of the *N*-glycan chains on the M1A1 and M1A2 domains appears to have decreased the amino acid backbone mobility resulting in an increased thermal stability as seen previously in other studies (22, 23). Although the removal of the glycosylation did not disrupt the secondary structure (as determined by CD), it is possible that the role of

FIGURE 5. **The effect of glycosylation of matrilin-1 A-domains on the binding to type II and IX collagen measured using QCM-D.** *A*, kinetics analysis of the binding between immobilized type II collagen and matrilin-3 and -1 A-domains in the presence of 1 mM Zn^{2+}. *B*, normalized frequency shift (mass change) and dissipation shift *versus* time, detected during the association of matrilin-1 and -3 A-domains onto immobilized type II collagen (*left panel*). The *right panel* represents normalized changes in ΔD as a function of Δf for data shown in the *left panel*. *C*, normalized frequency change and dissipation change *versus* time, detected during the association of matrilin-3 and -1 A-domains onto immobilized type IX collagen (*left panel*). The *right panel* shows the *D-f* plot using QCM-D raw data at the third overtone ($n = 3$).

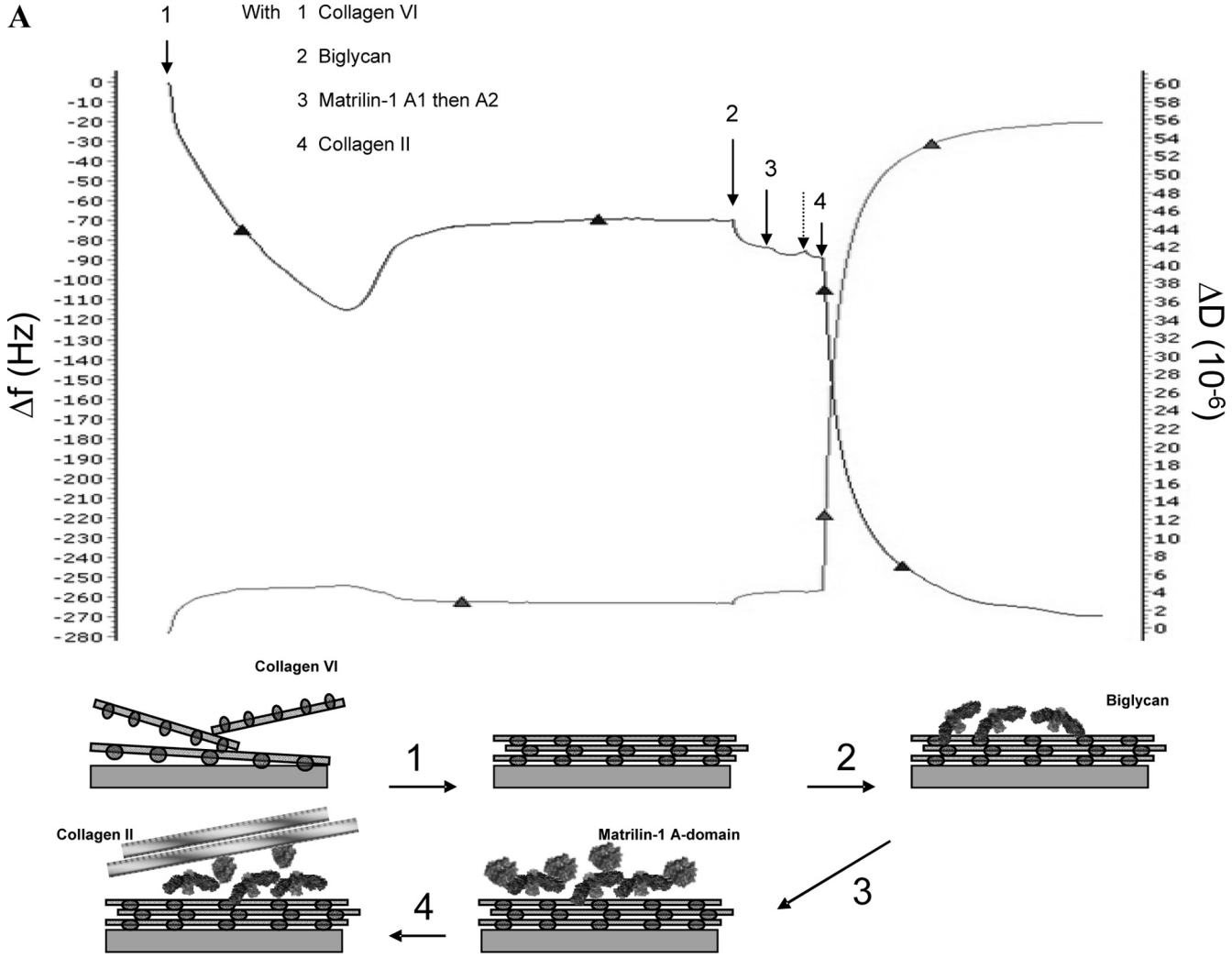
A
With 1 Collagen VI
2 Biglycan
3 Matrilin-1 A1 then A2
4 Collagen II
Δf (Hz)
ΔD (10-6)
Collagen VI
Biglycan
Collagen II
Matrilin-1 A-domain
1
2
3
4

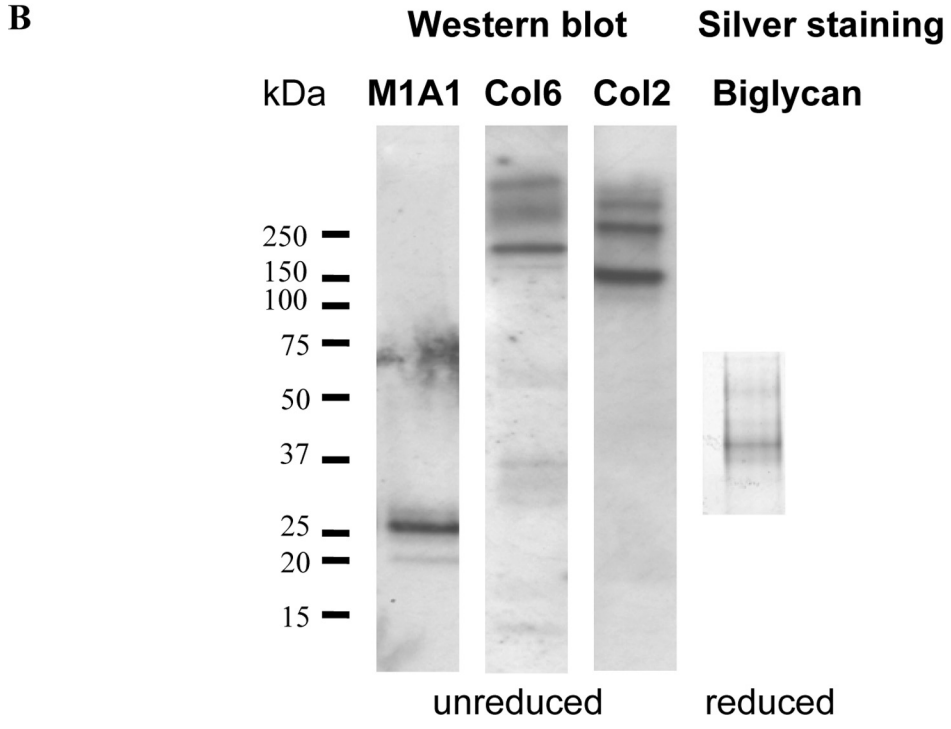
B
Western blot
Silver staining
kDa
M1A1
Col6
Col2
Biglycan
250
150
100
75
50
37
25
20
15
unreduced
reduced

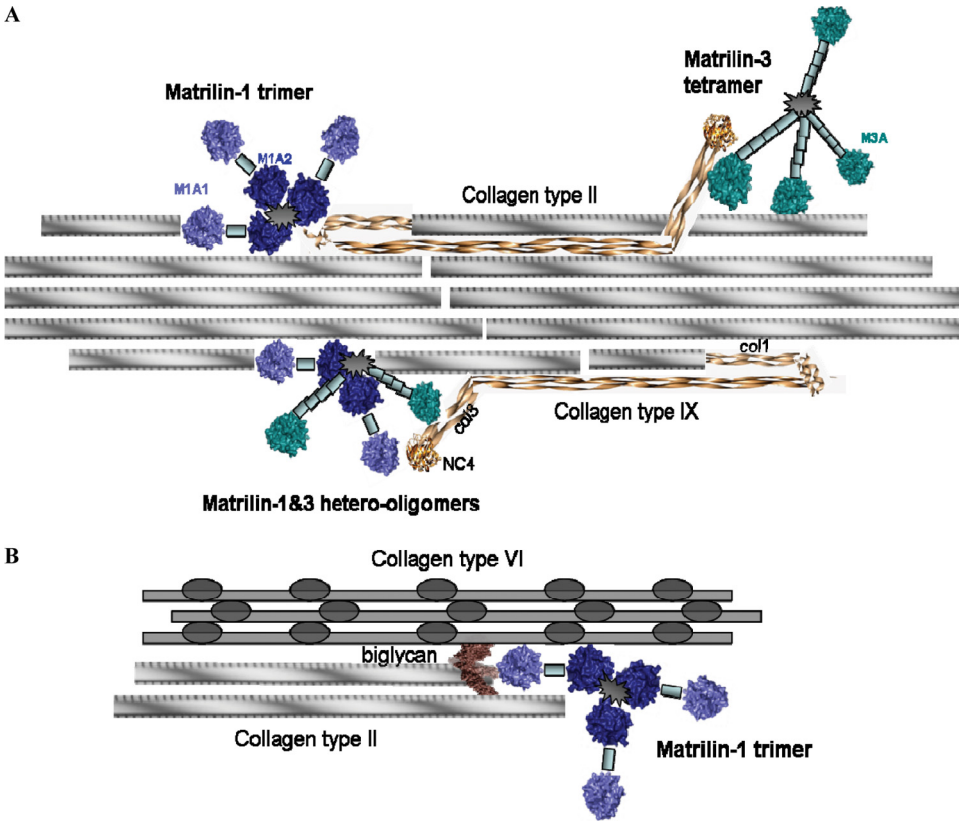

FIGURE 7. **Model of cartilage extracellular matrix assembly.** *A*, schematic of the protein complex formed between type II/IX collagen fibrils, matrilin-1 and matrilin-3 homo-oligomers, and matrilin-1/-3 hetero-oligomers. Protein pairing occurs preferentially between particular partners; *i.e.* the matrilin-3 A-domain binds to the COL3 domain of type IX collagen and along type II collagen fibrils compacting the architecture of the collagen network; whereas the M1A1 domain interacts at the end of the type II collagen fibrils and M1A2 domain binds to type IX collagen forming a "bridge" between type II and IX collagens. Matrilin-1/-3 hetero-oligomers further stabilizes the integrity of the cartilage ECM by combining these interactions pairing. *B*, schematic of the protein complex formed between type VI collagen microfibrils, biglycan, matrilin-1, and type II collagen.

glycosylation in the matrilin-1 A-domains has evolved after the structure was established. Indeed the highly conserved *N*-glycosylation sites were maintained in the chordate family with the exception of the distant zebrafish species. Glycosylation is known to act in an indirect manner by affecting the proteins intracellular trafficking. However, this was not the case for either the M1A1 or M1A2 domains because the unglycosylated proteins were both secreted into the cell culture medium. We therefore speculate that *N*-glycosylation could play a role in localization of the matrilin-1 protein in the cartilage extracellular matrix, thus explaining why matrilin-1 and unglycosylated matrilin-3 have different distributions in this tissue (6).

We also investigated a more direct role for *N*-glycosylation of both matrilin-1 A-domains as a potential physical barrier to, or an enhancer of, protein-protein interactions. Interestingly, by homology modeling the glycosylation sites are located at the opposite face of the MIDAS motif for the M1A1 domain, and on the side face of the molecule (α-2 helix) for M1A2. These specific locations have been described by Romijn *et al.* (24) to be the collagen-binding sites in two von Willebrand factors: namely VWF-A1 and VWF-A3, which share the highest structural homology to the matrilin-1 A-domains (Swiss Model data base). These collagen-binding sites are distinctly different from those of the integrin I-domain, another "A-domain" homologous to those of matrilin-1, where collagen binding occurs at the MIDAS motif (25).

We took advantage of the predicted location of the glycosylation on the M1A1 domain to determine whether it had any effect on the binding to collagen molecules. The unglycosylated variant of M1A1 bound with a significantly higher affinity to type II collagen compared with the wild type form ($p < 0.05$), which gave the domain a similar level of binding to that of M3A to which it shares a high sequence homology (62%) thereby suggesting they could have similar functions. This might help explain why the M3A domain lost its glycosylation potential during evolution (*i.e.* to facilitate the binding to collagen or to help modulate matrix assembly by ensuring there is a natural hierarchy in the binding process). From these experiments it cannot be concluded where the exact recognition site for type II collagen is located on the matrilin-1 A-domains because the interaction was not fully abolished by the presence or absence of the *N*-glycans chain. Further studies would need to be performed with the specific aim of mapping the binding sites on the collagen molecules and individual A-domains.

It has previously been determined that mutating a residue of the MIDAS motif in both of the matrilin-1 A-domains abolished filamentous network formation, suggesting that cations may be required for the function of matrilin-1 (9). Our binding studies performed in the presence of different cations established that Zn^{2+} participated actively in type II and IX collagen interactions by promoting binding and possibly exposing a binding surface that was formerly inaccessible. A previously published binding study performed between matrilin-1 and type II collagen in the presence of Ca^{2+} identified a much

FIGURE 6. **Complex formation between collagen type VI, biglycan, matrilin-1 A-domains, and collagen type II monitored in real-time using QCM-D.** *A*, monitoring of protein adsorption and supramolecular assembly by following the frequency change (Δf) and dissipation (ΔD) during deposition of a type VI collagen network (*1*), specific binding of biglycan (*2*), matrilin-1 A1 then A2 domains (*3*, *first arrow* is for M1A1 then the second for M1A2) and finally type II collagen (*4*). *B*, biochemical analysis of each component in the complex using Western blotting (specific antibodies against the FLAG tag of the matrilin-1 A1 domain, type VI and II collagens) and silver staining of biglycan.

weaker interaction (26). This suggests that both matrilin-1 A-domains have acquired specificity for Zn^{2+} binding, which is not unexpected because 85% of Zn^{2+} reserves are found in bone (27). Moreover, collation of Zn^{2+} was sufficient to abolish any binding, indicating that Zn^{2+} might be involved in activating the matrilin-1 A-domains and promoting their association with collagens in the ECM either through the MIDAS motif or elsewhere on the molecule (15). However, further experiments need to be performed to confirm any potential conformational changes of the matrilin-1 A-domains.

On the other hand, binding of matrilin A-domains might not occur at one unique recognition motif, but rather at several sites on the collagen molecule (28). Domains can be versatile in their binding properties and their association to specific ligands can be "loose and temporary" or "tight and permanent" (29). Protein-protein interactions are often casual association more than definite attachment and their specificity can be narrow, which is probably the case for the matrilin-1 and -3 A-domains. The first evidence for this variability in their binding properties was shown by Aszódi *et al.* (13) when they described a functionally redundant role for matrilin-1 and -3. Indeed, matrilin-1 or -3 null mice showed no overt skeletal phenotype suggesting that individually they are not critical for cartilage structure (14). However, matrilin-1 and -3-deficient mice have an abnormal type II collagen fibrillogenesis and fibril organization (30).

Our current data further confirm this compensatory mechanism between matrilin-1 and -3 biological functions. Both sets of kinetic data for type II collagen binding, performed on the SPR and the QCM-D, were in agreement by giving the same trend in binding affinity and confirmed that all three A-domains can potentially bind to type II collagen. The differences in the absolute K_D values might be due to the biological complexity of the interaction and the different orientation (matrilin A-domains were immobilized on the chip when using SPR, whereas the collagen type II was adsorbed on the crystal for the QCM-D experiments).

Similarly, all three matrilin A-domains were found to interact with type IX collagen. However, a tightening of the type IX collagen layer was only observed when the M3A domain came into contact with it. This observation suggests a novel functional role for the M3A domain as a bridging molecule compressing the cartilage collagen network. Interestingly, the matrilin-1 A-domains showed a similar structural change to that of M3A and type IX collagen when they came in contact with the type II collagen layer (by compacting its organization). In contrast, the M3A domain formed a more open and flexible complex when bound to the immobilized type II collagen surface.

Another example of the adaptability in binding of the matrilin-1 A-domains is their ability to bind to type VI collagen, unique among the collagen family in its molecular and fibrillar arrangement (19). We have shown for the first time the organizational hierarchy in real time of the type VI collagen-biglycan-matrilin-type II collagen complex, which is a key determinant of the chondrocyte territorial matrix.

In conclusion, all three matrilin-1/-3 A-domains are versatile in their binding to the structural collagen network of the cartilage ECM, with some slight nuances. 1) The M3A domain appears to preferentially bind to type IX collagen as previously suggested by Budde *et al.* (31) who demonstrated that the lack of type IX collagen resulted in a loss of matrilin-3 anchorage in the cartilage ECM. 2) The M1A domains show better affinity for type II collagen. This supports previous electron microscopy experiments in which matrilin-1 was seen to bind to both ends of type II collagen molecules (32). Indeed, findings from a matrilin-1 null mouse suggested that the lack of matrilin-1 in the matrix altered the structure of type II collagen fibrils (30). Our current working model illustrates that matrilin-1 A-domains are multivalent molecules that serve to connect different matrix components such as type VI collagen and biglycan in the chondrocyte territorial ECM, and that matrilin-1 and -3 A-domains stabilize and provide the "compacting" catalyst for the type II and IX collagen network in the inter-territorial ECM. This complex is regulated by slightly differing affinities of the different matrilin-1/-3 A-domains for the various components thus leading to a hierarchical preference. The increase in stability created by the glycosylation could help protect hetero-oligomers from degradation, whereas also providing some degree of tissue specificity. Finally, one of the possible roles for the matrilin-1 and -3 hetero-oligomers could be to further bring this collagen type II and IX integrated meshwork together by increasing their affinities to interact with the matrix (Fig. 7). The multivalency of matrilin-1/-3 A-domains brings essential molecules into close proximity, which in turn aids the three-dimensional structure of the ECM assembly and its overall stability.

Acknowledgments—We thank Prof. Paul Bishop (University of Manchester) for supplying biglycan and Dr. Debbie Krakow (Cedars-Sinai Medical Center) for making available full-length human matrilin-1 cDNA clones. We are also grateful to Emma Keevil for the mass spectrometry and Marj Howard for technical help with the light scattering.

REFERENCES

1. Paulsson, M., and Heinegård, D. (1979) *Biochem. J.* **183,** 539–545
2. Paulsson, M., and Heinegård, D. (1981) *Biochem. J.* **197,** 367–375
3. Wagener, R., Ehlen, H. W., Ko, Y. P., Kobbe, B., Mann, H. H., Sengle, G., and Paulsson, M. (2005) *FEBS Lett.* **579,** 3323–3329
4. Wu, J. J., and Eyre, D. R. (1998) *J. Biol. Chem.* **273,** 17433–17438
5. Klatt, A. R., Nitsche, D. P., Kobbe, B., Mörgelin, M., Paulsson, M., and Wagener, R. (2000) *J. Biol. Chem.* **275,** 3999–4006
6. Zhang, Y., and Chen, Q. (2000) *J. Biol. Chem.* **275,** 32628–32634
7. Kleemann-Fischer, D., Kleemann, G. R., Engel, D., Yates, J. R., 3rd, Wu, J. J., and Eyre, D. R. (2001) *Arch. Biochem. Biophys.* **387,** 209–215
8. Deák, F., Wagener, R., Kiss, I., and Paulsson, M. (1999) *Matrix Biol.* **18,** 55–64
9. Chen, Q., Zhang, Y., Johnson, D. M., and Goetinck, P. F. (1999) *Mol. Biol. Cell* **10,** 2149–2162
10. Frank, S., Schulthess, T., Landwehr, R., Lustig, A., Mini, T., Jenö, P., Engel, J., and Kammerer, R. A. (2002) *J. Biol. Chem.* **277,** 19071–19079
11. Zhang, Y., Wang, Z. K., Luo, J. M., Kanbe, K., and Chen, Q. (2008) *J. Orthop. Surg.* **3,** 21
12. Ehlen, H. W., Sengle, G., Klatt, A. R., Talke, A., Müller, S., Paulsson, M., and Wagener, R. (2009) *J. Biol. Chem.* **284,** 21545–21556
13. Aszódi, A., Bateman, J. F., Hirsch, E., Baranyi, M., Hunziker, E. B., Hauser, N., Bösze, Z., and Fässler, R. (1999) *Mol. Cell. Biol.* **19,** 7841–7845
14. Nicolae, C., Ko, Y. P., Miosge, N., Niehoff, A., Studer, D., Enggist, L., Hunziker, E. B., Paulsson, M., Wagener, R., and Aszodi, A. (2007) *J. Biol.*

Chem. **282,** 22163–22175
15. Fresquet, M., Jowitt, T. A., Ylöstalo, J., Coffey, P., Meadows, R. S., Ala-Kokko, L., Thornton, D. J., and Briggs, M. D. (2007) *J. Biol. Chem.* **282,** 34634–34643
16. Dixon, M. C. (2008) *J. Biomol. Tech.* **19,** 151–158
17. Whittaker, C. A., and Hynes, R. O. (2002) *Mol. Biol. Cell* **13,** 3369–3387
18. Dwek, R. A. (1995) *Biochem. Soc. Trans.* **23,** 1–25
19. Wiberg, C., Heinegård, D., Wenglén, C., Timpl, R., and Mörgelin, M. (2002) *J. Biol. Chem.* **277,** 49120–49126
20. Wiberg, C., Klatt, A. R., Wagener, R., Paulsson, M., Bateman, J. F., Heinegård, D., and Mörgelin, M. (2003) *J. Biol. Chem.* **278,** 37698–37704
21. Johansson, J. A., Halthur, T., Herranen, M., Söderberg, L., Elofsson, U., and Hilborn, J. (2005) *Biomacromolecules* **6,** 1353–1359
22. Tams, J. W., and Welinder, K. G. (2001) *Biochem. Biophys. Res. Commun.* **286,** 701–706
23. Ueda, T., Iwashita, H., Hashimoto, Y., and Imoto, T. (1996) *J. Biochem.* **119,** 157–161
24. Romijn, R. A., Westein, E., Bouma, B., Schiphorst, M. E., Sixma, J. J., Lenting, P. J., and Huizinga, E. G. (2003) *J. Biol. Chem.* **278,** 15035–15039
25. Springer, T. A. (2006) *Structure* **14,** 1611–1616
26. Mann, H. H., Ozbek, S., Engel, J., Paulsson, M., and Wagener, R. (2004) *J. Biol. Chem.* **279,** 25294–25298
27. Grennan, D. M., Knudson, J. M., Dunckley, J., MacKinnon, M. J., Myers, D. B., and Palmer, D. G. (1980) *N. Z. Med. J.* **91,** 47–50
28. Rich, R. L., Deivanayagam, C. C., Owens, R. T., Carson, M., Höök, A., Moore, D., Symersky, J., Yang, V. W., Narayana, S. V., and Höök, M. (1999) *J. Biol. Chem.* **274,** 24906–24913
29. Doolittle, R. F. (1995) *Annu. Rev. Biochem.* **64,** 287–314
30. Huang, X., Birk, D. E., and Goetinck, P. F. (1999) *Dev. Dyn.* **216,** 434–441
31. Budde, B., Blumbach, K., Ylöstalo, J., Zaucke, F., Ehlen, H. W., Wagener, R., Ala-Kokko, L., Paulsson, M., Bruckner, P., and Grässel, S. (2005) *Mol. Cell. Biol.* **25,** 10465–10478
32. Winterbottom, N., Tondravi, M. M., Harrington, T. L., Klier, F. G., Vertel, B. M., and Goetinck, P. F. (1992) *Dev. Dyn.* **193,** 266–276